




Loss-of-function variants in *C3ORF52* result in localized autosomal recessive hypotrichosis

Liron Malki, MSc^{1,2}, Ofer Sarig, PhD¹, Nicole Cesarato, MSc³, Janan Mohamad, PhD^{1,2}, Talia Canter, BS⁴, Sari Assaf, MSc^{1,2}, Mor Pavlovsky, MD¹, Dan Vodo, MD, PhD^{1,2}, Yossi Anis, PhD⁵, Ofer Bihari, PhD¹, Kiril Malovitski^{1,2}, Andrea Gat, MD¹, Holger Thiele, MD⁶, Bethany E. Perez White, PhD⁴, Liat Samuelov, MD¹, Arti Nanda, MD⁷, Amy S. Paller, MD, MSc⁴, Regina C. Betz, PhD³ and Eli Sprecher, MD, PhD^{1,2} 

Purpose: Localized autosomal recessive hypotrichosis (LAH) has been associated with pathogenic variants in *DSG4*, encoding a desmosomal protein as well as in *LIPH* and *LPAR6*, encoding respectively lipase H, which catalyzes the formation of 2-acyl-lysophosphatidic acid (LPA), and lysophosphatidic acid receptor 6, a receptor for LPA. LPA promotes hair growth and differentiation. In this study we aimed at delineating the genetic basis of LAH in patients without pathogenic variants in these three genes.

Methods: Variant analysis was conducted using exome and direct sequencing. We then performed quantitative reverse transcription polymerase chain reaction (RT-qPCR), immunofluorescence staining, immunoblotting, enzymatic, and coimmunoprecipitation assays to evaluate the consequences of potential etiologic variants.

Results: We identified homozygous variants in *C3ORF52* in four individuals with LAH. *C3ORF52* was found to be coexpressed with lipase H in the inner root sheath of the hair follicle and the two proteins were found to directly interact. The LAH-causing variants were associated with decreased *C3ORF52* expression and resulted in markedly reduced lipase H-mediated LPA biosynthesis.

Conclusion: LAH can be caused by abnormal function of at least three proteins which are necessary for proper LPA biosynthesis.

Genetics in Medicine (2020) 22:1227–1234; <https://doi.org/10.1038/s41436-020-0794-5>

Keywords: hair; hypotrichosis; alopecia; lipase H; *C3ORF52*

INTRODUCTION

Abnormal hair growth or density is often experienced as a psychologically devastating event, interfering with many aspects of affected individuals' personal and social life.¹ Targeted therapies for hair conditions are slowly emerging. In this regard, the study of inherited hair disorders has proven over recent years to be invaluable for deciphering novel aspects of hair follicle biology, which in turn may serve as the basis for the development of novel therapeutic approaches for rare as well as common hair conditions.

Hypotrichosis refers to a large group of disorders featuring sparse hair during early childhood.² Nonsyndromic hypotrichosis can be inherited in an autosomal dominant or autosomal recessive fashion³ and is characterized by extensive genetic heterogeneity.^{4–11} Localized autosomal recessive hypotrichosis (LAH) is a nonsyndromic form of hypotrichosis that typically features short, sparse, fragile hairs that break easily.¹² Three types of LAH have been described to date: LAH1 is caused by variants in *DSG4*¹² encoding a desmosomal protein (MIM 607903), LAH2 is caused by variants in *LIPH*⁸ encoding lipase H (MIM 607365), and

LAH3 is caused by variants in *LPAR6*⁹ (MIM 609239) encoding the lysophosphatidic acid receptor 6.

LAH2 and LAH3 share the same pathophysiology. Lipase H promotes the conversion of phosphatidic acid into lysophosphatidic acid (LPA), which then binds *LPAR6*, regulating a G protein-coupled receptor pathway that is essential for normal human hair formation.^{8,9,13} LPA affects hair follicle development through the epidermal growth factor receptor (EGFR) and the transforming growth factor (TGF)- α signaling pathways,¹⁴ eventually leading to the formation of hair keratins.^{15,16}

In the present study, we describe the identification of a novel LAH-associated gene, broadening our understanding of the physiological mechanisms regulating human hair growth and pointing to novel therapeutic targets for the treatment of hypotrichoses and related disorders.

MATERIALS AND METHODS

Patients

The patients and their healthy family members provided informed consent to participate in this study according to

¹Division of Dermatology, Tel Aviv Sourasky Medical Center, Tel Aviv, Israel; ²Department of Human Molecular Genetics & Biochemistry, Sackler Faculty of Medicine, Tel Aviv University, Ramat Aviv, Israel; ³Institute of Human Genetics, University of Bonn, School of Medicine and University Hospital Bonn, Bonn, Germany; ⁴Department of Dermatology, Northwestern University Feinberg School of Medicine, Chicago, Illinois, USA; ⁵Institute of Endocrinology, Tel Aviv Sourasky Medical Center, Tel Aviv, Israel; ⁶Cologne Center for Genomics, University of Cologne, Cologne, Germany; ⁷As'ad Al-Hamad Dermatology Center, Kuwait, Kuwait. Correspondence: Eli Sprecher (elisp@tlvmc.gov.il)

Submitted 19 November 2019; accepted: 26 March 2020

Published online: 27 April 2020

protocols approved by institutional review boards at the recruiting institutions (Northwestern University Feinberg School of Medicine, Chicago, IL, USA and As'ad Al-Hamad Dermatology Center, Kuwait). Consent to publish patient photos was obtained from the patients' legal guardians.

Cell cultures

Primary keratinocytes were obtained as previously described¹⁷ and maintained in keratinocyte growth medium (KGM; Lonza, Walkersville, MD, USA). HeLa cells were kindly provided by Mia Horowitz (Tel-Aviv University, Israel). Cells were maintained in Dulbecco's Modified Eagle Medium (DMEM) 4.5 g/l glucose medium containing 10% fetal calf serum (FCS), 1% L-glutamine, and 1% penicillin and streptomycin and grown at 37 °C and 5% CO₂ (Biological Industries, Beit-Haemek, Israel). HEK293T cells were maintained in DMEM 4.5 g/l glucose medium (Lonza) containing 10% fetal bovine serum (FBS) and 1% penicillin and streptomycin and grown at 37 °C and 5% CO₂.

Antibodies

The following antibodies were used: mouse monoclonal anti-V5 epitope tag (Invitrogen, Carlsbad, CA, USA, R960-25); rabbit polyclonal anti-LIPH (Proteintech, Rosemont, IL, USA, 16602-1-AP); rabbit polyclonal anti-C3orf52 (Thermo Fisher Scientific, Waltham, MA, USA; PA552889); mouse monoclonal anti-LIPH (Proteintech, 66303-1-Ig); rabbit anti-PDI (Abcam, ab3672); antimouse Cy3 (Invitrogen, A10521); antirabbit AlexaFluor647 (A-21244, Invitrogen); rhodamine red X goat polyclonal antimouse secondary antibody (Invitrogen, Carlsbad, CA, USA, R-6393); and DyLight 488 goat polyclonal antirabbit secondary antibody (Invitrogen, Carlsbad, CA, USA, 35553).

Exome sequencing

Exome sequencing in family 1 was performed by Fulgent Genetics Ltd. Exome capture was carried out by in-solution hybridization with Roche Nimblegen Protocol (10 GB) followed by massively parallel sequencing (Illumina HiSeq4000) with 150-bp paired-end reads. Reads were aligned to the Genome Reference Consortium Human Build 37 (GRCh37/hg19) using Burrows–Wheeler.¹⁸ Duplicate reads, resulting from polymerase chain reaction (PCR) clonality or optical duplicates, and reads mapping to multiple locations were excluded from downstream analysis. Reads mapping to a region of known or detected insertions or deletions were realigned to minimize alignment errors. Single-nucleotide substitutions and small insertion deletions were identified and quality filtered using the Genome Analysis Tool Kit (GATK).¹⁹ Rare variants were identified by ANNOVAR²⁰ and filtered using data from dbSNP142, the 1000 Genomes Project, Human Gene Mutation Database (HGMD), gnomAD, Ensemble, Exome Variant Server, and an in-house database of individual exomes. Variants were classified by predicted protein effects using PolyPhen-2,²¹ SIFT,²² Pro-vean,²³ ConSeq,²⁴ and MutationTaster.²⁵ Exome sequencing

in family 2 was performed at CCG (Cologne, Germany). First, 1 µg of DNA was sonicated, and the fragments subjected to end repair and adapter ligation. After size selection, the libraries were enriched with the SeqCap EZ Human Exome Library version 2.0 kit (Roche NimbleGen, Madison, WI). The libraries were then sequenced using a paired-end protocol and an Illumina HiSeq 2000 (Illumina, San Diego, CA), as described elsewhere.²⁶ Data filtering and analysis were performed using the varbank pipeline v.2.18.

Validation and cosegregation of the disease phenotype with the variant were verified using Sanger sequencing. Table S1 summarizes exome sequencing details.

Direct sequencing

Genomic DNA was PCR-amplified using oligonucleotide primer pairs spanning the coding sequence as well as intron–exon boundaries of *C3ORF52* (Table S2) with Taq polymerase (Qiagen, Hilden, Germany). Cycling conditions were as follows: 98 °C, 2 minutes; 96 °C, 30 seconds; 62 °C, 30 seconds; 72 °C, 30 seconds, for 30 cycles, 72 °C 10 minutes. Gel-purified (QIAquick gel extraction kit, QIAGEN, Hilden, Germany) amplicons were subjected to bidirectional DNA sequencing with the BigDye terminator system on an ABI Prism 3100 sequencer (Applied Biosystems, Foster City, NY, USA) with the same oligonucleotides used for PCR amplification.

Plasmid synthesis and mutagenesis

A synthetic *C3ORF52* (NM_024616.2) complementary DNA (cDNA) construct with a C-terminal V5-tag and a synthetic *LIPH* (NM_139248.3) cDNA with a C-terminal HA-tag were cloned into pcDNA3.1 plasmids (Epoch Life Science, USA). To incorporate p.Tyr164Ter and p.Glu12Ter variants, mutagenesis primers were generated with the use of the New England Biolabs Inc., NEBaseChanger® (<http://nebasechanger.neb.com>) and are provided in Table S3. The procedure was performed with the use of the Q5® Site-Directed Mutagenesis Kit (New England Biolabs Inc.) according to the manufacturer's instructions. Construct sequence and insert orientation were verified by Sanger sequencing using the primers reported in Table S4.

Quantitative RT-PCR

For quantitative real-time PCR (qRT-PCR), cDNA was synthesized from 1000 ng of total RNA using qScript kit (Quanta Biosciences, Gaithersburg, MD, USA). cDNA PCR amplification was carried out with the PerfeCTa SYBR Green FastMix (Quanta Biosciences, Gaithersburg, MD, USA) on a StepOnePlus system (Applied Biosystems, Waltham, MA, USA) with gene-specific intron-crossing oligonucleotides (provided in Table S5). Cycling conditions were as follows: 95 °C, 20 seconds, followed by 95 °C, 3 seconds; 60 °C, 30 seconds for 40 cycles. Each sample was analyzed in triplicates. For each set of primers, standard curves were obtained with serially diluted cDNAs. Results were normalized to *GAPDH* messenger RNA (mRNA) levels.

Protein extraction

Forty-eight hours after transfection with a total of 10 µg of each plasmids, HeLa cells, cultured in 10 mm plates, were lysed in CelLytic™ MT (Sigma-Aldrich, St. Louis, MO, USA) in the presence of a protease inhibitor mix, including 1 mM phenylmethanesulfonylfluoride, and 1 mg ml⁻¹ aprotinin and leupeptin (Sigma-Aldrich). The amount of protein in each sample was determined with the Pierce™ BCA Protein Assay Kit (Thermo Fisher) according the manufacturer's instructions.

Coimmunoprecipitation assay

Following centrifugation at 10,000g for 10 minutes at 4 °C, cell lysates were immunoprecipitated with the use of SureBeads protein G magnetic beads (Bio-Rad, Hercules, CA, USA; catalog #161-4023) according to the manufacturer's instructions. SureBeads protein G magnetic beads were incubated, prior to immunoprecipitation, with a mouse monoclonal anti-V5 epitope tag antibody (Invitrogen, Carlsbad, CA, USA; catalog #R960-25; 8 µg/sample) for three hours and immunoprecipitation was performed overnight at 4 °C.

Western blotting

Eluted proteins were electrophoresed through 12.5% sodium dodecyl sulfate–polyacrylamide gel electrophoresis (SDS-PAGE) and transferred onto a nitrocellulose membrane (Trans-Blot, Bio-Rad). After blocking for 1 hour using 1 × TBST (50 mM Tris, 150 mM NaCl, 0.01% Tween 20) with 3% bovine serum albumin (BSA), blots were incubated overnight at 4 °C with a primary polyclonal rabbit anti human-LIPH (diluted 1:1000, Proteintech, catalog #16602-1-AP). The blots were washed 5 times for 5 minutes each with 1 × TBST with 1.5% BSA. After incubation with a secondary horseradish peroxidase–conjugated antirabbit antiserum (diluted 1:5000; Sigma-Aldrich) and subsequent washings (5 times for 5 minutes each with 1 × TBST), proteins were detected using the EZ-ECL chemiluminescence detection kit (Biological Industries, Beit-Haemek, Israel).

Tissue immunofluorescence staining

For immunofluorescence analysis of skin biopsies, 5 µm paraffin-embedded sections were deparaffinized using xylene/ethanol; antigen retrieval was performed with 0.01 M citrate buffer, pH 6.0 (Invitrogen) in a microwave for 25 minutes and blocked with 2% BSA in phosphate-buffered saline (PBS) for 30 minutes at room temperature. The sections were incubated overnight at 4 °C with a rabbit anti-C3ORF52 primary antibody (PA552889, Thermo Fisher) diluted 1:200 or 1:50 with 2% BSA in PBS or a mouse monoclonal anti-LIPH antibody (Proteintech, 66303-1-Ig) diluted 1:200 with 2% BSA in PBS. Secondary staining was carried out for 45 minutes at 37 °C using rhodamine red X antimouse and Dylight 488 antirabbit secondary antibodies diluted 1:200 (Life Technologies/Invitrogen). Coverslips were mounted in DAPI Fluoromount-G (Southern Biotechnologies, Birmingham,

AL, USA). Imaging was performed using an LSM 700 confocal microscope (Zeiss, Germany).

Cell immunofluorescence staining

Immunofluorescence analysis was performed in triplicates on transiently transfected HEK293T cells grown on poly-L-lysine solution 0.01% (Sigma-Aldrich) treated coverslips. Cells were fixed with paraformaldehyde 4% and then permeabilized with PBS-Tween 20 for 10 minutes. After blocking with BSA supplemented with 1% normal goat serum for 1 hour, cells were incubated with mouse monoclonal anti-V5 antibody (1:500) and rabbit anti-PDI (1:600) for an additional hour. This was followed by incubation for 40 minutes with the secondary antibodies antimouse Cy3 (1:500) and antirabbit AlexaFluor647 (1:600) with addition of DAPI (Invitrogen). Slides were then mounted with Mowiol and images were generated with the Leica CytoVision DM5500B and the Cytovision 7.4 software. The procedure was performed in triplicates.

Lipase H activity assay

HeLa cells were cotransfected with wild-type *LIPH* and with either wild-type or the mutated *C3ORF52* constructs. An empty vector served as negative control. Forty-eight hours after transfection, cells were lysed in CelLytic™ MT (Sigma-Aldrich) in the presence of a protease inhibitor mix, including 1 mM phenylmethanesulfonylfluoride, and 1 mg ml⁻¹ aprotinin and leupeptin (Sigma-Aldrich). The amount of protein was determined with the Pierce™ BCA Protein Assay Kit (Thermo Fisher). Then, 5 µg of total protein was diluted into 100 µl of Hanks' balanced salt solution (HBSS) buffer containing 0.5 µM PED-A1 (N-[(6-[2,4-DNP]amino)hexanoyl]-1-[BODIPY®FL C₅]-2-hexyl-*sn*-glycero-3-phosphoethanolamine; Invitrogen, catalog #A10070). PED-A1 comprises a quencher group (dinitrophenyl) on the glycerophosphoethanolamine head group and BODIPY dye-labeled acyl chains at the sn-1 position. Cleavage of the molecule by lipase H increases green fluorescence by uncoupling the quenched state. Phospholipase activity was monitored every 120 seconds for 2 hours at 24 °C using the Tecan Infinite M200 Reader (excitation filter 485 nm, emission filter 535 nm).

Quantification of endogenous TGF-α release from human keratinocyte cells

Human keratinocyte cells were seeded in 12-well plates (100,000 cells per well) and cultured for 2 days up to 60% confluency, and were then transfected with *C3ORF52* wild-type or variant expression vectors using a total of 500 ng DNA and Lipofectamine 2000 (Invitrogen) according to the manufacturer's instructions. An empty vector served as blank control. Twenty-four hours after transfection medium was replaced with KGM (Walkersville, MD, USA) containing 1.5 mM CaCl₂ followed by 48 hours incubation to induce differentiation and to be used for TGF-α release experiment. Media were concentrated by using Amicon Ultra-4

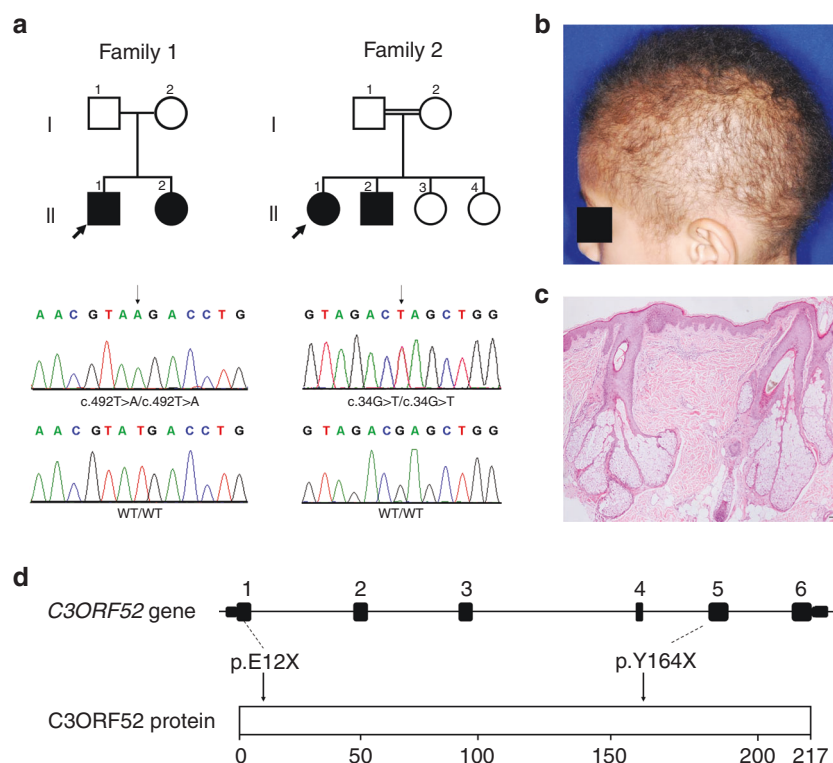


Fig. 1 Clinical features and variant analysis. (a) Pedigrees of the two families. Black symbols denote affected individuals. Direct sequencing of *C3ORF52* (NM_024616.2) revealed a homozygous T>A transversion (arrow) at position c.492 of the complementary DNA (cDNA) sequence in individuals II-1 and II-2, family 1 (middle left panel) as well as a homozygous G>T transversion (arrow) at position c.34 of the cDNA sequence in individuals II-1 and II-2, family 2 (middle right panel). The wild-type sequences (WT/WT) are given for comparison (lower panels). (b) Hypotrichosis in individual II-1, family 1. (c) Histopathological examination of a scalp skin biopsy obtained from individual II-2, family 1 demonstrates decreased hair density in the absence of inflammation and fibrosis (scale bar, 100 μ m). (d) The location of the two variants is depicted along a schematic representation of the *C3ORF52* gene and C3ORF52 protein.

Centrifugal Filters (Sigma-Aldrich) and TGF- α levels in conditioned media were measured with a TGF- α sandwich enzyme-linked immunosorbent assay (ELISA) (human TGF- α DuoSet Kit, R&D Systems) according to the manufacturer's instructions. Optical density at 450 nm and 570 nm was measured with a Tecan Infinite M200 absorbance reader.

RESULTS

Genetic variant analysis

We studied four individuals with LAH (Fig. 1a, b). The first two patients were born to healthy, unrelated parents of Hispanic descent (Fig. 1a; family 1, II-1 and II-2) and showed isolated scalp hypotrichosis. The other two patients were born to healthy first-degree cousins of Arab Muslim descent (Fig. 1a; family 2, II-1 and II-2) and displayed involvement of the scalp, eyebrows, and eyelashes. Histopathological examination of a skin biopsy obtained from the scalp of patient II-2, family 1 revealed decreased hair follicle density with predominance of vellus hair follicles with no evidence of inflammation or fibrosis (Fig. 1c).

All affected and healthy family members or their legal guardians provided written and informed consent to participate in this study. To delineate the genetic basis of LAH in the

two families, DNA samples obtained from individual II-1, family 1, and from individual II-1, family 2, were used for exome sequencing (ES, Table S1). Two homozygous nonsense variants in *C3ORF52* (NM_024616.2) were found to cosegregate with the disease phenotype in both families: c.492T>A in family 1 and c.34G>T in family 2 (Fig. 1a; Fig. S1). Both variants result in a premature termination codon (p. Tyr164Ter and p. Glu12Ter respectively). The c.34G>T variant was absent from all public databases, while variant c.492T>A was present in a heterozygous state in 1 of 119,840 individuals in the gnomAD database. Both variants are predicted to be damaging by prediction software with a Combined Annotation Dependent Depletion (CADD) score of 33 (c.492T>A) and 35 (c.34G>T), which indicates that the variants are among the top 0.1% of the deleterious variants in the human genome.

C3ORF52 consists of six coding exons and an open reading frame of 217 amino acids. Although *C3ORF52* function is unknown, it is expressed predominantly in skin²⁷ (Fig. S2). *C3ORF52* expression was strongest in the inner root sheath (IRS) of the hair follicle (Fig. S3). The IRS ensures proper molding, adherence, and keratinization of the growing hair shaft.²⁸

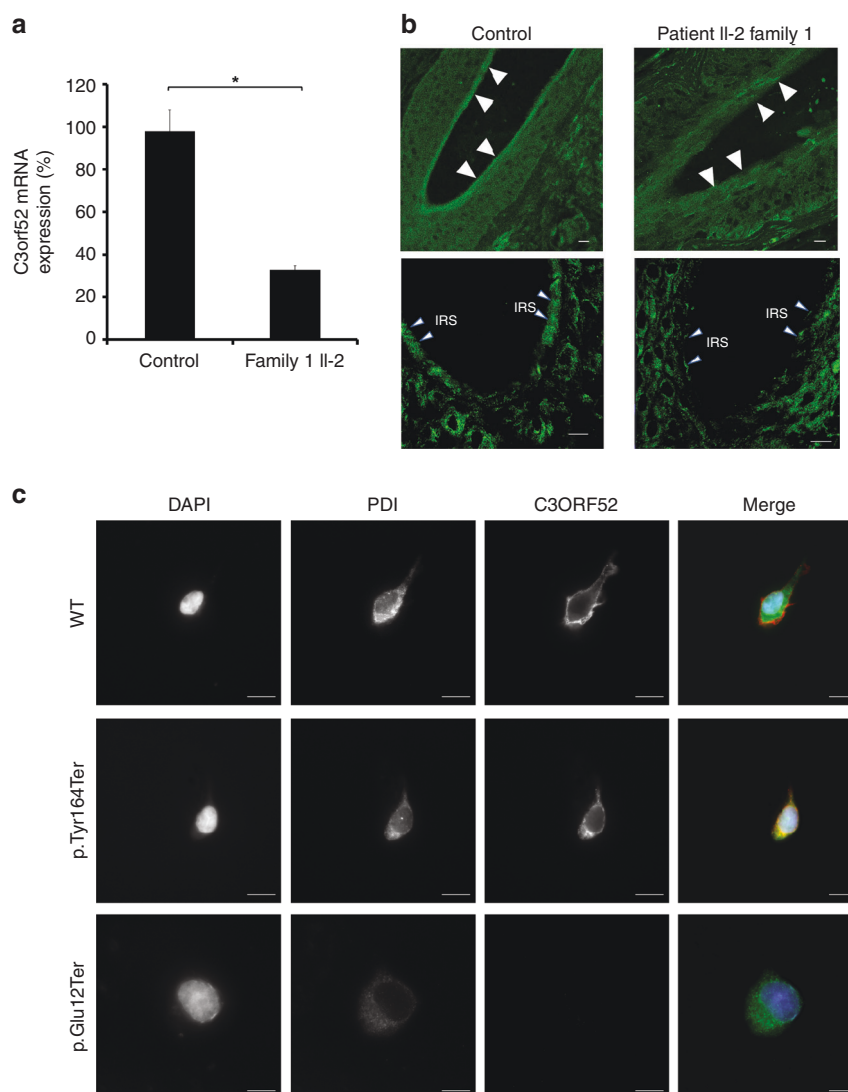


Fig. 2 Consequences of localized autosomal recessive hypotrichosis (LAH)-causing variants in *C3ORF52*. (a) Real-time polymerase chain reaction (PCR) analysis was used to quantify *C3ORF52* RNA expression using complementary DNA (cDNA) derived from keratinocytes obtained from two healthy individuals (control, comparison was done separately) and patient II-2, family 1 (patient). Results are expressed as percentage of RNA expression relative to expression in control samples \pm standard error of the mean (two sided *t* test; $*p < 0.05$). Results are normalized to *GAPDH* RNA levels. (b) Scalp skin biopsy samples obtained from patient II-2, family 1 and from a healthy person (control) were stained with an anti-*C3ORF52* antibody (scale bar, 10 μ m). Lower (upper panel) and higher (lower panel) magnifications are shown. Staining is prominent along the inner root sheath (IRS) in the control but not in the patient (arrowheads). (c) HEK293T cells transiently expressing wild-type or mutant *C3ORF52* were stained with 4,6-diamidino-2-phenylindole-dihydrochloride (DAPI, blue staining) and antibodies against V5 (*C3ORF52* and mutants, red staining), and protein disulfide isomerase (PDI, green staining) (scale bar, 10 μ m). *C3ORF52* wild type is located in the cell membrane, whereas the mutant protein carrying p.Tyr164Ter is located predominantly in the endoplasmic reticulum (green staining) and the mutant protein carrying p.Glu12Ter cannot be detected. *mRNA* messenger RNA.

Consequences of *C3ORF52* variants

Using RT-qPCR and RNA isolated from keratinocyte cultures derived from a skin biopsy obtained from patient II-2, family 1, *C3ORF52* mRNA levels were found to be markedly reduced (Fig. 2a). Accordingly, immunostaining showed downregulation of *C3ORF52* expression in a scalp skin sample obtained from patient II-2, family 1 (Fig. 2b). In addition, in contrast with wild-type *C3ORF52*, which was found to be expressed along the cell membrane, p.Tyr164Ter-carrying *C3ORF52* was found to colocalize with an endoplasmic reticulum marker (disulfide isomerase, PDI), suggesting that this variant

results not only in decreased *C3ORF52* expression but also in protein mislocalization (Fig. 2c). The p.Glu12Ter variant was associated with absence of *C3ORF52* protein (Fig. 2c).

C3ORF52 functional analysis

Lipase H is responsible for catalyzing the transformation of phosphatidic acid into LPA, which upon binding to the LPAR6 receptor drives hair follicle morphogenesis through modulation of the TGF α -EGFR signaling pathway.^{14,15} Of interest, lipase H, like *C3ORF52*, is also mainly expressed in the IRS¹⁴ and *C3ORF52* has previously been

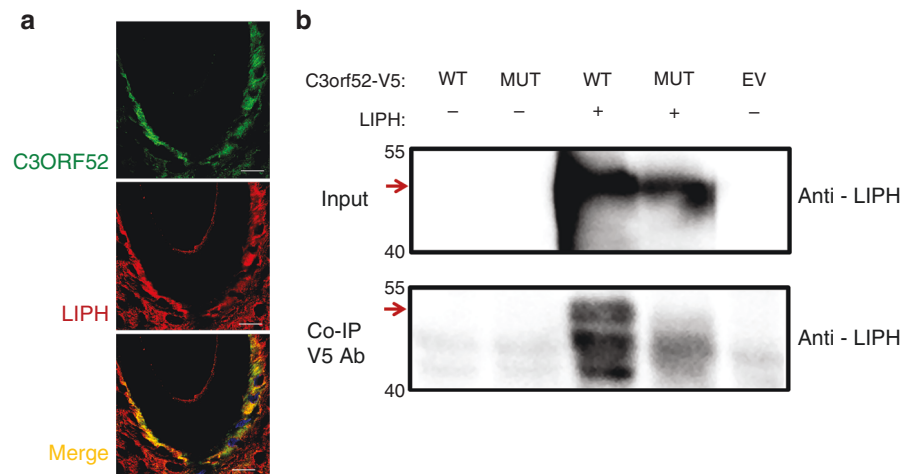


Fig. 3 *C3ORF52* association with lipase H. (a) Normal skin scalp biopsies were stained with an anti-*C3ORF52* antibody (green) and with an anti-lipase H antibody (red). Both proteins were observed to partially colocalize along the inner root sheath area (merge) (scale bar, 10 μm; blue staining, DAPI); negative controls are shown in Fig. S4. (b) Coimmunoprecipitation (Co-IP) assay using proteins extracted from HeLa cells cotransfected with *LIPH* and with V5-tagged *C3ORF52* (wild-type [WT] or mutated [MUT, carrying the p.Tyr164Ter variant]). Protein extracts (input) were immunoprecipitated with a mouse monoclonal anti-V5 epitope tag antibody bound to protein G SureBeads and resolved by western blot. Protein–protein interactions were immunodetected using an anti-*LIPH* antibody. Protein blot shows a signal at about 51 kD, corresponding to the size anticipated for the lipase H protein (indicated by a red arrow). Cell lysates from HeLa cells transfected with either a pcDNA3.1 empty vector (EV) or with the wild-type or the mutated C-terminus V5-tagged *C3ORF52* alone served as controls. The experiment was repeated twice with similar results. The original coimmunoprecipitation images are shown in Fig. S5.

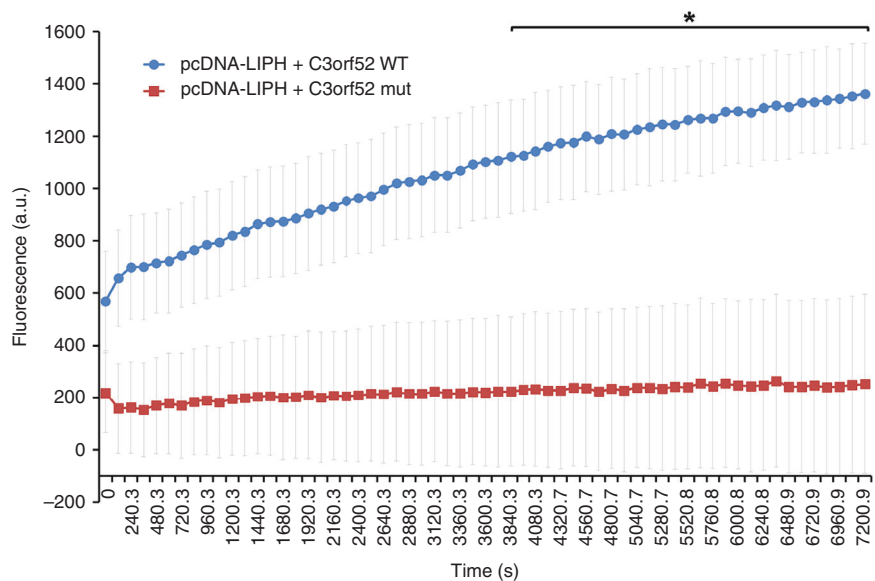


Fig. 4 Lipase H activity in HeLa cells transfected with wild-type (WT) lipase H and either wild-type or variant *C3ORF52* was measured as detailed in Supplementary Materials and Methods. Fluorescence emission at 535 nm, reflecting lipase H activity, was monitored every 120 seconds for 2 hours, immediately upon adding the PED-A1 substrate. Fluorescence data are expressed as arbitrary units (a.u.). Data represent the mean values \pm standard deviation (SD) of four independent experiments done in duplicates (time series regression; $*p < 0.05$). Background values recorded from extracts of HeLa cells transfected with a pcDNA3.1 empty vector were subtracted from the experimental readings.

suggested to interact with lipase H based on data extracted from BioPlex 2.0 (Biophysical Interactions of ORFeome-derived complexes).^{29,30} Moreover, the InterMine³¹ tool fed through the GenesLikeMe software³² predicts that *C3ORF52* and lipase H may be involved in common lipid metabolism-associated pathways (see Table S6), suggesting that *C3ORF52* may functionally interact with lipase H in the hair follicle.

Supporting this possibility, immunostaining of normal skin biopsies revealed colocalization of *C3ORF52* and lipase H to the IRS (Fig. 3a and Fig. S4). Coimmunoprecipitation assays using proteins extracted from HeLa cells transfected with *C3ORF52* and *LIPH* further suggested an association between *C3ORF52* and lipase H (Fig. 3b), which was not detectable when cells were cotransfected with a *C3ORF52* construct carrying the LAH-causing c.492T>A variant (Fig. 3b).

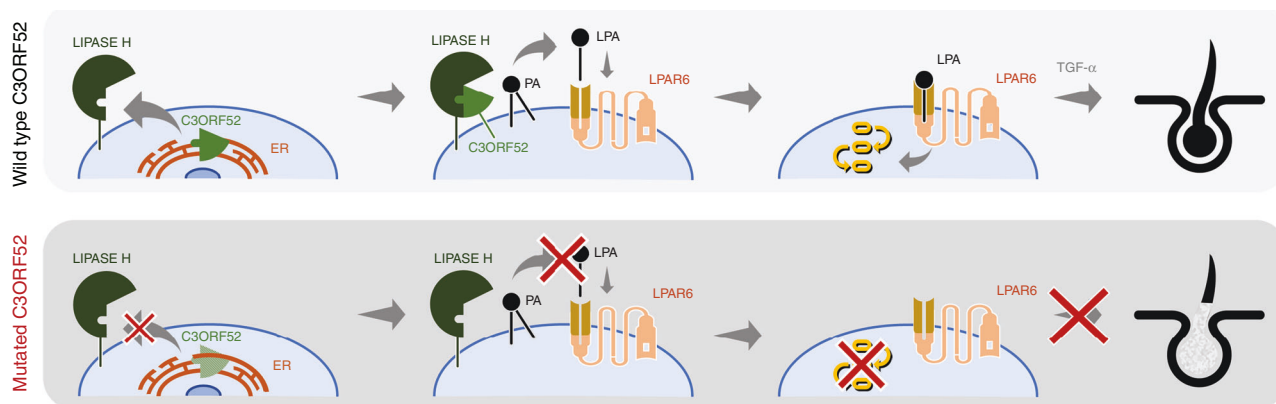


Fig. 5 Mechanism of action of C3ORF52. A scheme summarizing the proposed mechanism of action of C3ORF52 (upper panel) and the consequences of the localized autosomal recessive hypotrichosis (LAH)-associated variants (lower panel) is shown. Briefly, under normal circumstances (upper panel), after binding of C3ORF52, lipase H is able to catalyze the transformation of phosphatidic acid (PA) into acyl-lysophosphatidic acid (LPA). LPA then binds to the LPAR6 receptor, which drives hair follicle morphogenesis through upregulation of TGF- α release. In the absence of functional C3ORF52 (lower panel), lipase H ability to catalyze LPA formation is impaired, and as a consequence TGF- α is not released, and hair growth is abnormal.

To ascertain the functional significance of C3ORF52 interaction with lipase H, we measured LPA production in cells cotransfected with *LIPH*, and wild-type *C3ORF52* or c.492T>A-carrying-*C3ORF52* (see Supplementary Material and Methods). Lipase H-mediated LPA biosynthesis was markedly inhibited in the presence of the mutant C3ORF52 as compared with wild-type protein indicating that C3ORF52 is required for normal lipase H-mediated LPA biosynthesis (Fig. 4).

As mentioned above, TGF- α mediates the hair follicle growth-promoting activity of LPA.¹³ We therefore compare TGF- α levels in keratinocytes transfected with wild-type versus variant C3ORF52. As shown in Fig. S6, transfection with the variant C3ORF52 resulted in a dramatic reduction in TGF- α release levels (Fig. S6).

DISCUSSION

Hair loss can have psychologically devastating effects in young patients and their relatives.³³ In this regard, the study of monogenic hair disorders is of particular importance as it often uncovers novel therapeutic targets of relevance to those as well as related conditions. The deciphering of the pathogenesis of atrichia with papular lesions (MIM209500) and of hypotrichosis simplex of scalp type 1 (MIM 607479) remarkably illustrates this paradigm as it has demonstrated in a clinical setting the importance of WNT signaling for normal hair development,^{5,34} which in turn has formed the basis for pilot studies of novel hair growth-promoting therapies.^{35,36} Similarly, the identification of pathogenic variants in *LIPH*⁸ and *LPAR6*¹³ in multiple families with LAH has demarcated a new biological pathway ultimately leading to the biosynthesis of LPA^{14,15} (which may possibly intersect with the WNT/ β -catenin signaling pathway¹⁶) and critical for the maintenance of hair growth.³⁷ The present study attributes to C3ORF52, a protein to date without a known function, a pivotal role in this pathway as C3ORF52 seems to be necessary for normal LPA biosynthesis (Fig. 5).

Not only are lipase H, C3ORF52, and LPAR6 equally important for proper hair growth, LPA biosynthesis seems to require their colocalization to the cell membrane,^{13,38} as demonstrated by the fact that absence of membrane expression of C3ORF52 was sufficient to prevent normal LPA production (Fig. 5).

LAH is part of a steadily growing number of monogenic hair disorders resulting from abnormal lipid biosynthesis or transport³⁹ as exemplified by pathogenic variants in *LSS* encoding lanosterol synthase, an important enzyme in the cholesterol pathway, associated with hypotrichosis simplex,⁷ and by loss-of-function pathogenic variants in the *ABCA5* gene resulting in hypertrichosis due to decreased cholesterol efflux and intracellular accumulation of cholesterol.⁴⁰

The fact that all three proteins defective in LAH are critical for proper LPA biosynthesis and the fact that phosphatidic acid and LPA were shown to promote hair follicle formation in mice^{15,41} point to these molecules as potential therapeutic targets for LAH and possibly other hair disorders.

SUPPLEMENTARY INFORMATION

The online version of this article (<https://doi.org/10.1038/s41436-020-0794-5>) contains supplementary material, which is available to authorized users.

ACKNOWLEDGEMENTS

This work was supported in part by a generous donation of the Ram family (E.S.), the German-Israeli Foundation (E.S. and R.C.B.), and by the Deutsche Forschungsgemeinschaft (DFG, German Research Foundation) under Germany's Excellence Strategy—EXC2151–390873048 (R.C.B.). We are grateful to the Northwestern University Skin Biology and Diseases Resource-based Center (P30 AR075049) for assistance with the materials from family 1. We thank Deborah Rapaport for insightful discussions and the patients and their families for participating to this study.

DISCLOSURE

The authors declare no conflicts of interest.

Publisher's note Springer Nature remains neutral with regard to jurisdictional claims in published maps and institutional affiliations.

REFERENCES

- Williamson D, Gonzalez M, Finlay AY. The effect of hair loss on quality of life. *J Eur Acad Dermatol Venereol*. 2001;15:137–139.
- Betz RC, Cabral RM, Christiano AM, Sprecher E. Unveiling the roots of monogenic genodermatoses: genotrichoses as a paradigm. *J Invest Dermatol*. 2012;132:906–914.
- Ahmed A, Almohanna H, Griggs J, Tosti A. Genetic hair disorders: a review. *Dermatol Ther* (Heidelb). 2019;9:421–448.
- Levy-Nissenbaum E, Betz RC, Frydman M, et al. Hypotrichosis simplex of the scalp is associated with nonsense mutations in CDSN encoding corneodesmosin. *Nat Genet*. 2003;34:151–153.
- Shimomura Y, Agalliu D, Vonica A, et al. APCDD1 is a novel Wnt inhibitor mutated in hereditary hypotrichosis simplex. *Nature*. 2010;464:1043–1047.
- Pasternack Sandra M, Refke M, Paknia E, et al. Mutations in SNRPE, which encodes a core protein of the spliceosome, cause autosomal-dominant hypotrichosis simplex. *Am J Hum Genet*. 2013;92:81–87.
- Romano M-T, Tafazzoli A, Mattern M, et al. Bi-allelic mutations in LSS, encoding lanosterol synthase, cause autosomal-recessive hypotrichosis simplex. *Am J Hum Genet*. 2018;103:777–785.
- Kazantseva A, Goltsov A, Zinchenko R, et al. Human hair growth deficiency is linked to a genetic defect in the phospholipase gene LIPH. *Science*. 2006;314:982–985.
- Shimomura Y, Wajid M, Ishii Y, et al. Disruption of P2RY5, an orphan G protein-coupled receptor, underlies autosomal recessive woolly hair. *Nat Genet*. 2008;40:335–339.
- Zernov NV, Skoblov MY, Marakhonov AV, et al. Autosomal recessive hypotrichosis with woolly hair caused by a mutation in the keratin 25 gene expressed in hair follicles. *J Invest Dermatol*. 2016;136:1097–1105.
- Zhou C, Zang D, Jin Y, et al. Mutation in ribosomal protein L21 underlies hereditary hypotrichosis simplex. *Hum Mutat*. 2011;32:710–714.
- Schaffer JV, Bazzi H, Vitebsky A, et al. Mutations in the desmoglein 4 gene underlie localized autosomal recessive hypotrichosis with monilethrix hairs and congenital scalp erosions. *J Invest Dermatol*. 2006;126:1286–1291.
- Pasternack SM, von Kügelgen I, Al Aboud K, et al. G protein-coupled receptor P2Y5 and its ligand LPA are involved in maintenance of human hair growth. *Nat Genet*. 2008;40:329–334.
- Inoue A, Arima N, Ishiguro J, Prestwich GD, Arai H, Aoki J. LPA-producing enzyme PA-PLA(1)α regulates hair follicle development by modulating EGFR signalling. *EMBO J*. 2011;30:4248–4260.
- Lei L, Su J, Chen J, Chen W, Chen X, Peng C. The role of lysophosphatidic acid in the physiology and pathology of the skin. *Life Sci*. 2019;220:194–200.
- Raza SI, Muhammad D, Jan A, et al. In silico analysis of missense mutations in LPAR6 reveals abnormal phospholipid signaling pathway leading to hypotrichosis. *PLoS ONE*. 2014;9:e104756.
- Nousbeck J, Ishida-Yamamoto A, Bidder M, et al. IGFBP7 as a potential therapeutic target in psoriasis. *J Invest Dermatol*. 2011;131:1767–1770.
- Li H, Durbin R. Fast and accurate long-read alignment with Burrows-Wheeler transform. *Bioinformatics*. 2010;26:589–595.
- McKenna A, Hanna M, Banks E, et al. The Genome Analysis Toolkit: a MapReduce framework for analyzing next-generation DNA sequencing data. *Genome Res*. 2010;20:1297–1303.
- Wang K, Li M, Hakonarson H. ANNOVAR: functional annotation of genetic variants from high-throughput sequencing data. *Nucleic Acids Res*. 2010;38:e164.
- Adzhubei IA, Schmidt S, Peshkin L, et al. A method and server for predicting damaging missense mutations. *Nat Methods*. 2010;7:248–249.
- Kumar P, Henikoff S, Ng PC. Predicting the effects of coding non-synonymous variants on protein function using the SIFT algorithm. *Nat Protoc*. 2009;4:1073–1081.
- Choi Y, Sims GE, Murphy S, Miller JR, Chan AP. Predicting the functional effect of amino acid substitutions and indels. *PLoS ONE*. 2012;7:e46688.
- Ashkenazy H, Erez E, Martz E, Pupko T, Ben-Tal N. ConSurf 2010: calculating evolutionary conservation in sequence and structure of proteins and nucleic acids. *Nucleic Acids Res*. 2010;38:W529–533.
- Schwarz JM, Cooper DN, Schuelke M, Seelow D. MutationTaster2: mutation prediction for the deep-sequencing age. *Nat Methods*. 2014;11:361–362.
- FB UB, Cau L, Tafazzoli A, et al. Mutations in three genes encoding proteins involved in hair shaft formation cause uncombable hair syndrome. *Am J Hum Genet*. 2016;99:1292–1304.
- Fagerberg L, Hallström BM, Oksvold P, et al. Analysis of the human tissue-specific expression by genome-wide integration of transcriptomics and antibody-based proteomics. *Mol Cell Proteomics*. 2014;13:397–406.
- Harland DP. Introduction to hair development. *Adv Exp Med Biol*. 2018;1054:89–96.
- Huttlin EL, Bruckner RJ, Paulo JA, et al. Architecture of the human interactome defines protein communities and disease networks. *Nature*. 2017;545:505–509.
- Huttlin EL, Ting L, Bruckner RJ, et al. The BioPlex Network: a systematic exploration of the human interactome. *Cell*. 2015;162:425–440.
- Smith RN, Aleksic J, Butano D, et al. InterMine: a flexible data warehouse system for the integration and analysis of heterogeneous biological data. *Bioinformatics*. 2012;28:3163–3165.
- Stelzer G, Inger A, Olender T, et al. GeneDecks: paralog hunting and gene-set distillation with GeneCards annotation. *OMICS*. 2009;13:477–487.
- Liu LY, King BA, Craiglow BG. Alopecia areata is associated with impaired health-related quality of life: a survey of affected adults and children and their families. *J Am Acad Dermatol*. 2018;79:556–8 e551.
- Thompson CC, Sisk JM, Beaudoin GM 3rd. Hairless and Wnt signaling: allies in epithelial stem cell differentiation. *Cell Cycle*. 2006;5:1913–1917.
- Tosti A, Zaiac MN, Canazza A, et al. Topical application of the Wnt/β-catenin activator methyl vanillate increases hair count and hair mass index in women with androgenetic alopecia. *J Cosmet Dermatol*. 2016;15:469–474.
- Jo SJ, Shin H, Park YW, et al. Topical valproic acid increases the hair count in male patients with androgenetic alopecia: a randomized, comparative, clinical feasibility study using phototrichogram analysis. *J Dermatol*. 2014;41:285–291.
- Shimomura Y. Congenital hair loss disorders: rare, but not too rare. *J Dermatol*. 2012;39:3–10.
- Hiramatsu T, Sonoda H, Takanezawa Y, et al. Biochemical and molecular characterization of two phosphatidic acid-selective phospholipase A1s, mPA-PLA1α and mPA-PLA1β. *J Biol Chem*. 2003;278:49438–49447.
- Stenn KS, Karnik P. Lipids to the top of hair biology. *J Invest Dermatol*. 2010;130:1205–1207.
- DeStefano GM, Kurban M, Anyane-Yeboah K, et al. Mutations in the cholesterol transporter gene ABCA5 are associated with excessive hair overgrowth. *PLoS Genet*. 2014;10:e1004333.
- Takahashi T, Kamimura A, Hamazono-Matsuoka T, Honda S. Phosphatidic acid has a potential to promote hair growth in vitro and in vivo, and activates mitogen-activated protein kinase/extracellular signal-regulated kinase in hair epithelial cells. *J Invest Dermatol*. 2003;121:448–456.